

ON THE USE OF ANGLED, DYNAMIC LASER BEAMS TO IMPROVE STEREOLITHOGRAPHY SURFACE FINISH

Benay Sager and David W. Rosen

The Woodruff School of Mechanical Engineering
Georgia Institute of Technology
Atlanta, GA 30332-0405

Reviewed, accepted August 31, 2004

ABSTRACT

Improved surface finish of Stereolithography (SLA) parts is an important goal for furthering the resolution of the technology. In order to improve the surface finish, a dynamic laser beam with changing angle, beam size, beam shape, and irradiance distribution is proposed. In this paper, an analytical irradiance model of an angled, dynamic laser beam in the SLA process is presented. This model is used to simulate cured shapes of SLA builds. Simulated build shapes are compared to established SLA analytical models and conclusions are drawn on the accuracy of the developed model.

1. INTRODUCTION AND MOTIVATION FOR STUDY

Stereolithography (SLA) is a layered rapid prototyping process in which an UltraViolet (UV) laser is used to selectively cure a vat of liquid photopolymer resin in order to physically fabricate a part from a CAD model. With the growing interest in applying this technology to the microfabrication area comes the need to study the resolution of SLA. More specifically, the limits of the resolution, both theoretical and empirical, need to be established.

At the core of the SLA process is the UV laser or light source. The irradiance profile of this light source is the determining factor of cured SLA profile shapes. Traditional SLA systems use a stationary UV laser with galvanometer-driven mirrors to scan a particular cross-section on the build surface. For modeling purposes, some general behavior of the laser beam has been widely assumed. While this general behavior is a simplified form of the laser beam characteristics, it does not reflect the dynamic nature of the SLA build process, and hence resulting cured parts. These assumptions about the behavior of the laser beam during the SLA build process, as presented by [1, 2] and others and its characteristics are presented in Table 1.

Table 1. Analytical Modeling Assumptions for SLA Laser Beam

Area	Traditional SLA Models' Assumption	Dynamic Model (presented here)
Beam diameter	Beam has constant diameter and circular shape	Beam size and shape changes according to location on surface
Beam irradiance	Constant irradiance profile	Irradiance profile changes depending on the point of focus
Beam angle	Laser beam is always perpendicular to build surface	Laser beam angle with vertical changes during scanning
Refraction	Refraction does not affect cure profile	Refraction changes size, shape, and location of cure profile

As shown in Table 1, traditional SLA laser beam modeling assumes that the laser beam has a constant diameter and irradiance profile, and is always perpendicular to the build surface. For SLA modeling that involves changing laser beam parameters, especially in micro-scale applications, it is imperative to know the exact cure profile, so that the resolution of the technology can be quantified and improved. Even though in traditional systems the laser beam

deviates slightly from the vertical, it is still important to model the laser beam irradiance analytically in an accurate fashion.

Moreover, it has been shown that generating better upfacing surface finish is possible by changing the angle of the build surface while keeping the laser stationary [3, 4]. The outline of a SLA cured shape can be quantified with one of the surface finish parameters such as surface roughness or cusp height. It is possible to express the cusp height as a relationship between the angle of the surface, the angle of the build, and the layer thickness that is used. This relationship between the cusp height and the layer thickness is shown in Figure 1.

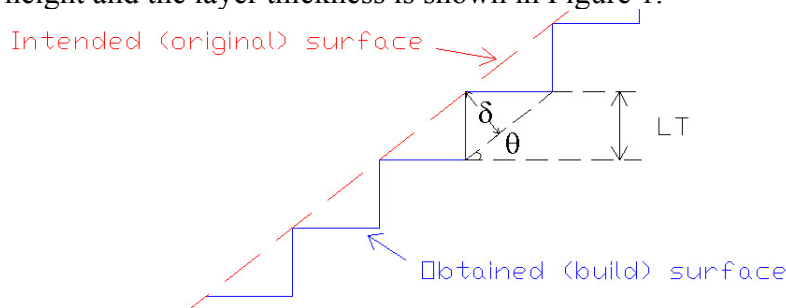


Figure 1. Relationship between layer thickness and cusp height

In Figure 1 the cusp height between the intended and obtained build surface is denoted by δ , whereas the angle of the intended surface is shown by θ . The angle θ can be used to approximate the surface finish i.e. cusp height for a given layer thickness. The relationship between this angle and the expected cusp height for upfacing surfaces is given as $\delta = LT \cos \theta$ [3]. The typical variation of surface roughness with respect to this angle for upfacing surfaces is presented in Figure 2.

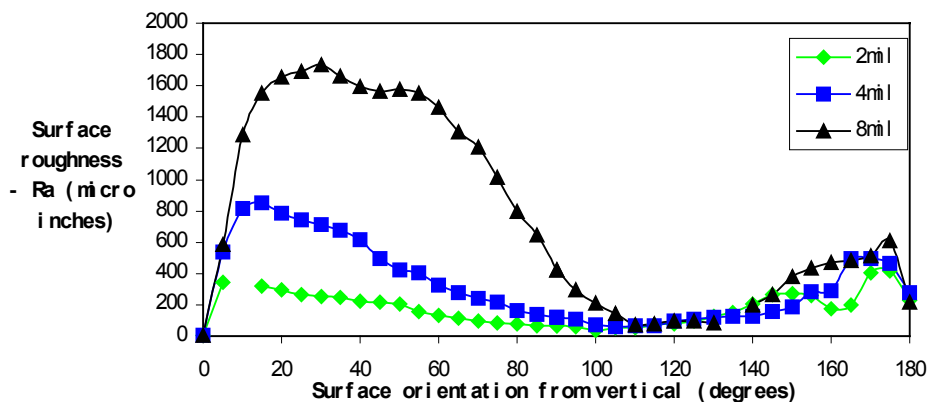


Figure 2. Cusp height versus build orientation [5] [3]

In Figure 2, the variation of surface roughness with respect to surface orientation is given for SLA 250 machine. When θ is small (between 0 and 15 degrees), the angle between the laser beam and vertical is large *but* attainable surface roughness is very small, which results in better surface finish.

In order to truly improve SLA surface finish, a more adaptive laser beam needs to be used during the build process. By enabling direct control of laser beam angle, different cure profiles can be obtained. Cure profiles with varying sizes and shapes can then be used to improve the surface finish of an SLA part feature via better surface approximation [6]. Even though no

commercial SLA machines with active laser beam angle control exist, we believe that such machines can be designed. Therefore, it is important to model the laser beam irradiance profile analytically so that such a model can be extended to micro-scale applications with changing laser beam build angles, helping predict the shape of the cured profiles *before* they are built.

2. ANALYTICAL SLA IRRADIANCE MODEL

For the purposes of this study, the irradiance distribution of an SLA laser is modeled as Gaussian. Irradiance is the radiant power of the laser per unit area (mW/cm^2), and is often denoted by $H(x,y,z)$. A Gaussian beam always either diverges from or converges to a point. However, because of diffraction, converging to a single point does not occur [7]. Instead, the beam does reach a minimum value, d_o , the beam waist diameter. For a Gaussian laser beam, the irradiance has its peak value at the beam waist. The beam waist for a Gaussian laser beam propagating along the z direction is shown in Figure 3. The beam waist is dependent on other laser beam variables such as divergence angle and wavelength in the following fashion:

$$d_o = \frac{4\lambda}{\pi\theta_b} \quad (\text{Equation 1})$$

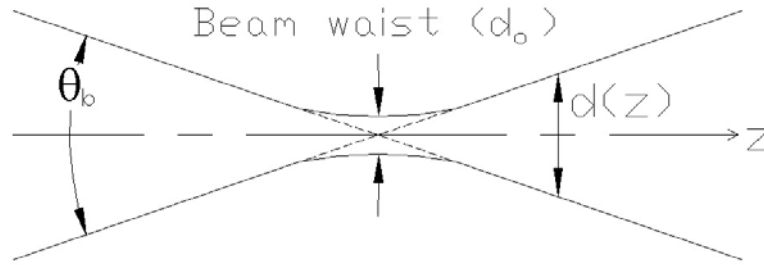


Figure 3. Gaussian laser beam waist

It is also useful to characterize the extent of the beam waist region with a parameter called the Rayleigh range, which is the distance from the beam waist where the diameter has increased to $\sqrt{2}d_o$. The collimated region of a Gaussian beam waist is equal to $2z_R$ [7]. The Rayleigh range is calculated as:

$$z_R = \frac{d_o}{\theta_b} = \frac{4\lambda}{\pi\theta_b^2} = \frac{\pi d_o^2}{4\lambda} \quad (\text{Equation 2})$$

The irradiance at any given point along a laser beam depends on the radial and perpendicular distances d and z away from the beam waist. The irradiance is a function of the maximum irradiance H_o that occurs at beam waist. Irradiance is given by [7]:

$$H(d,z) = \frac{H_o \exp\left(-\left(\frac{2d^2}{d_o^2}\right)\right)}{1 + \left(\frac{z^2}{z_R^2}\right)} \quad (\text{Equation 3})$$

The maximum irradiance can be determined by integrating the irradiance function over the area covered by the beam at this point. This integral must equal the laser power that is used in the particular SLA machine, P_L . Then,

$$H_o = \frac{8P_L}{\pi d_o^2} \quad (\text{Equation 4})$$

What is important for characterization of the laser beam is how irradiance changes along the SLA vat. The irradiance is affected by two main factors: distance away from beam waist, and the angle between laser beam and vertical. In order to take these two factors into account, it is more convenient to use a spherical coordinate system.

2.1 SLA Spherical Coordinate System

SLA parts are manufactured by scanning the laser beam in the x and y directions using two galvanometer-driven low inertia mirrors. Even though the mirrors rotate, the center point of the second mirror does not change significantly. Therefore, the second mirror can be taken as the origin point of the laser beam. In essence, by choosing the second mirror as the origin point of the laser beam, the origin of the spherical coordinate axis is selected at a point with height h above the center of the build surface. The correlation between the conventional Cartesian vat coordinate system and the spherical coordinate system is shown in Figure 4.

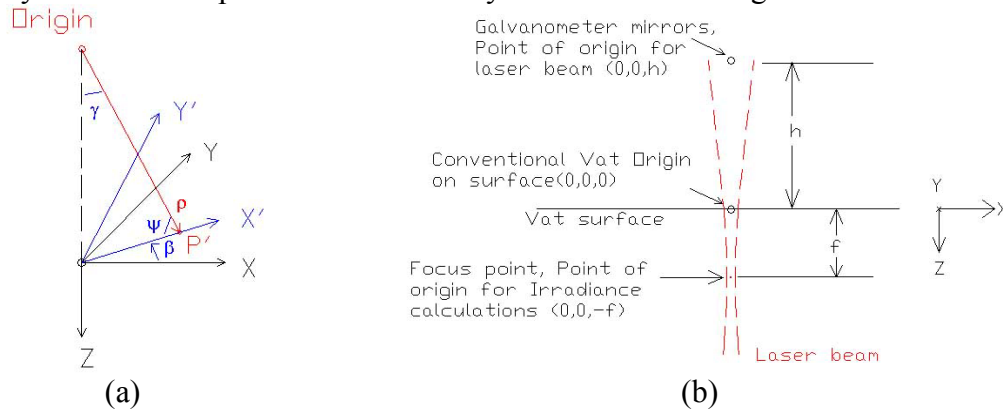


Figure 4. Coordinate systems used (a) Origin of systems (b) Origin with laser beam

In Figure 4a, the origin of the Cartesian coordinates is the center of the vat surface, (0,0,0). The spherical coordinate system is defined by ρ, β, ψ in Figure 4a, where ρ is the spherical distance away from point (0,0,h). The axis X' makes an angle β with axis X . The angle ψ is between the galvanometer mirror and axis X' , and angle $\gamma = 90 - \psi$ from basic geometry. The focus depth f in Figure 4b into the resin is the location of the theoretical beam waist, and is typically 3mm[8]. For any point P with coordinates (x_p, y_p, z_p) in the vat, the general conversion to spherical coordinates ρ, β, γ is as follows:

$$P(x_p, y_p, z_p) \equiv P(\rho_p, \beta_p, \gamma_p) = \left(\sqrt{x_p^2 + y_p^2 + (z_p + h)^2}, \tan^{-1}(y_p / x_p), \pi / 2 - \left(\tan^{-1}((z_p + h) / \sqrt{x_p^2 + y_p^2}) \right) \right) \quad (\text{Equation 5})$$

The location of the beam waist along the laser beam is constant, and it is at a radial distance $\rho_f = (h + f)$. However, the angle that the focus point makes with the vertical, γ_F , will change accordingly, as the beam moves around the build surface. The point where the center of the laser

beam intersects the vat surface, $F(x_F, y_F, 0)$ forms the basis for several irradiance calculations [1] and its spherical coordinates are given as:

$$F(\rho_F, \beta_F, \gamma_F) = \left(\sqrt{x_F^2 + y_F^2 + h^2}, \tan^{-1}(y_F / x_F), \frac{\pi}{2} - \tan^{-1}\left(h / \sqrt{x_F^2 + y_F^2}\right) \right) \quad (\text{Equation 6})$$

2.2 Refraction and Absorption Effects

In the SLA process, the path of the laser beam is refracted inside the resin, resulting in a change of the location of the theoretical beam waist within the resin. It can be assumed that the maximum angle made with the surface of the resin is not large enough to result in a significant percentage of the laser beam to be reflected. However, the Beer-Lambert absorption law is assumed to be valid for the SLA [9, 10] process. The effects of refraction within the resin are shown in Figure 5.

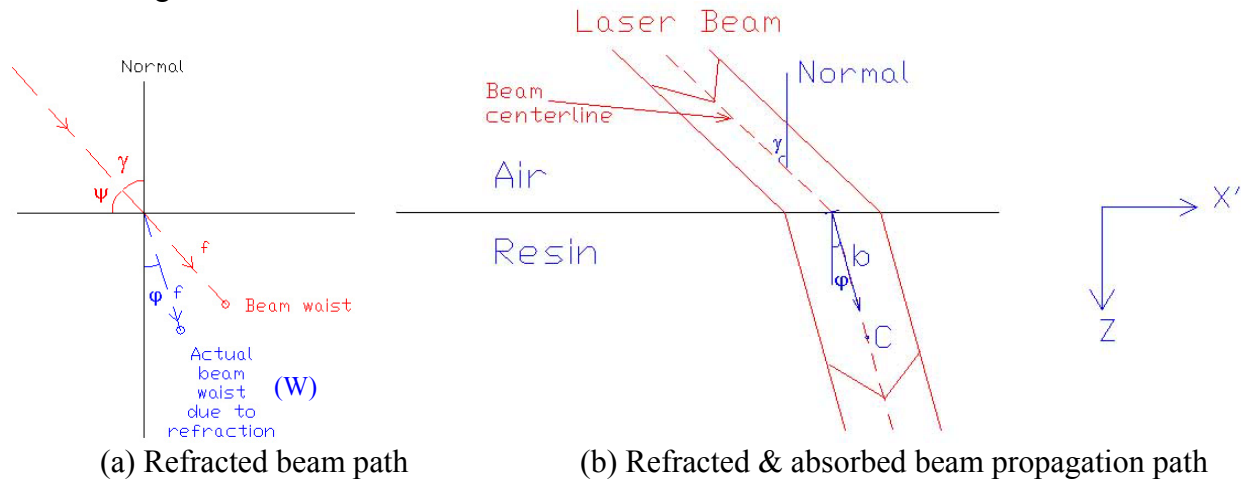


Figure 5. Effect of refraction on laser beam within vat

As shown in Figure 5a, using Snell's law for refraction, the relationship between the incident and refractive beam angles can be established. For air, the refractive index can be taken as 1. For SLA resins, the refractive index is estimated to be 1.5 [11]. It can be assumed that the refractive index of SLA resins does not change significantly over time and refractive index of cured and uncured resin are similar. Therefore, the path of refracted laser beam is given as:

$$\varphi = \sin^{-1}(\sin \gamma_F / 1.5) \quad (\text{Equation 7})$$

In Figure 5b, the path of the laser beam makes an angle γ_F with the normal before hitting the resin surface. The beam progresses along the direction b, refracted path. The irradiance along this path reaches up to the point C, which is the maximum depth of travel achieved by the laser beam within the vat. The Beer-Lambert law for the SLA process is:

$$H = H_{\text{surface}} \exp(-g / D_p) \quad (\text{Equation 8})$$

where $g = \|z_p / \cos \varphi\|$ is the length of the laser beam attenuation path along the refracted ray and D_p is the depth of penetration, a resin constant.

2.3 Irradiance Calculation for Arbitrary Point in Vat

There are 2 distinct cases for calculating SLA irradiance within the vat, as shown in Figure 6. For scans close to the center of the vat, the *theoretical* beam waist is within the vat. This is Case 1. The reason why the beam waist is theoretical in Case 1 is because the focus depth (3mm) in SLA is much larger than the typical depth of penetration (0.25mm). Therefore, the laser beam never penetrates deep enough into the resin as a result of absorption. For scans that are at the corners of the vat, the *actual* beam waist is either on or above the vat surface, constituting Case 2.

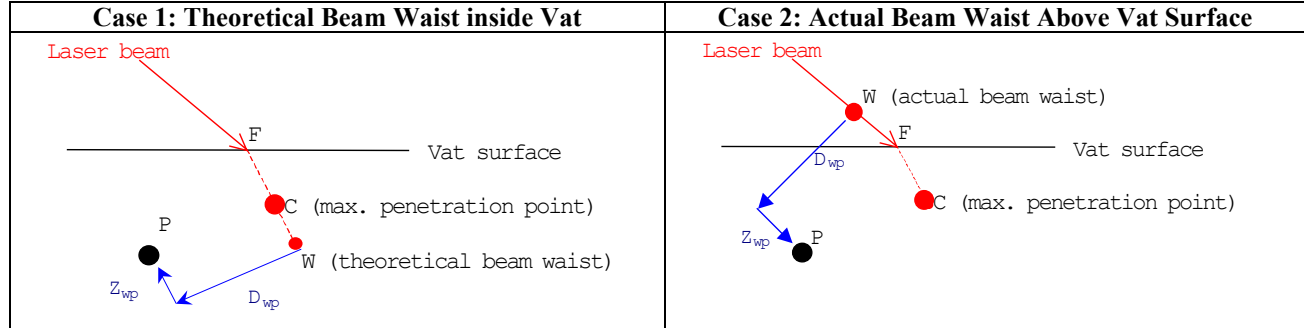


Figure 6. Summary of Cases for Beam Waist Location Determination

Calculating the location of the beam waist, W , is essential in determining the irradiance at any given point inside the vat. However, the method for calculation of beam waist location is different for the 2 cases. To determine which case is at hand, the distance between the beam waist location and the point F must be found:

$$\Delta_F = \rho_f - \rho_F \quad (\text{Equation 9})$$

If the quantity Δ_F is larger than zero, then the beam waist location falls inside the vat (Case 1). Otherwise, Case 2 occurs. For each case, the location of W (x_w, y_w, z_w) can be determined relative to the point F on the build surface where the center of the laser beam intersects the build surface. For Case 1, since the path of the laser beam will be along the axis X' , the location of the beam waist inside the vat is given as:

$$W_{case1}(x_w, y_w, z_w) = \left(\left(\sqrt{x_F^2 + y_F^2} + \Delta_F \sin \varphi \right) \cos \beta_F, \left(\sqrt{x_F^2 + y_F^2} + \Delta_F \sin \varphi \right) \sin \beta_F, \Delta_F \cos \varphi \right) \quad (\text{Equation 10})$$

In Case 2, the path of W in spherical coordinates is the same as the path of the focus point F . Since the spherical coordinates of F are known, the spherical coordinates of the theoretical beam waist can be expressed as:

$$W_{case2}(\rho_w, \beta_w, \gamma_w) = (\rho_F + \Delta_F, \beta_F, \gamma_F) \quad (\text{Equation 11})$$

Through some algebraic manipulation, the Cartesian coordinates of W for Case 2 are obtained as:

$$W_{case2}(x_w, y_w, z_w) = (\rho_w \sin \gamma_w \cos \beta_w, \rho_w \sin \gamma_w \sin \beta_w, \rho_w \cos \gamma_w - h) \quad (\text{Equation 12})$$

To calculate irradiance at any arbitrary point using Equation 3, the distances between P and W that are parallel and perpendicular to the beam propagation path must be found. In short, the distances Z_{wp} and D_{wp} in Figure 6 need to be calculated. In this context, the distance D_{wp} refers to

the shortest distance between the line FW and point P (d in Equation 3), whereas the distance Z_{wp} (z in Equation 3) refers to the distance between points W and P parallel to the beam path of FW. These parameters are computed as follows [12]:

$$\vec{M} = \vec{F} - \vec{W} \quad (\text{Equation 13})$$

$$t = \frac{\vec{M} \bullet (\vec{P} - \vec{F})}{\vec{M} \bullet \vec{M}} \quad (\text{Equation 14})$$

$$\vec{D}_{wp} = \vec{P} - (\vec{F} + t\vec{M}) \quad (\text{Equation 15})$$

$$Z_{wp} = \left\| (\vec{P} - \vec{W}) - \vec{D}_{wp} \right\| \quad (\text{Equation 16})$$

Inserting the calculated parameters into Equation 3 yields the irradiance equation for point P:

$$H(P) = \frac{H_o \exp\left(\frac{-\left(\frac{2\|D_{wp}\|^2}{d_o^2}\right)}{1 + \left(\frac{Z_{wp}^2}{z_R^2}\right)}\right) \exp\left(-\frac{g}{D_p}\right)}{1 + \left(\frac{Z_{wp}^2}{z_R^2}\right)} \quad (\text{Equation 17})$$

It should be noted that in Case 2, the path of refraction within the resin could be accounted for in the irradiance equation by adding a constant. However, the deviation of the refracted beam path from propagation of the laser beam is not significant enough within the Rayleigh range to merit this. Therefore, this effect is ignored.

The irradiance model was developed so that it can be used to predict cure profiles. To do so, the exposure at any point in the vat needs to be known. Exposure is defined as the integral of irradiance at a point over time:

$$E(x, y, z) = \int_{t_{start}}^{t_{end}} H[x(t), y(t), z(t)] dt \quad (\text{Equation 18})$$

3. APPLICATION OF ANALYTICAL IRRADIANCE MODEL

The analytical model has been applied to generate irradiance profile measurements for points within the vat. In addition, it has been used to simulate the cured profile shape of line scans. In this section, the results of both the irradiance and exposure simulations will be presented. These simulations were implemented in Matlab.

3.1 Irradiance Model Simulation

The developed irradiance model is comprehensive in the sense that it takes dynamic beam characteristics and refraction into account. This model, as presented in Equation 17, was used to generate an overall irradiance profile around a focus point in the vat. This was done for the

SLA250/50 machine, which has laser power of 35 mW, beam diameter of 0.25mm, and wavelength of 325 nm. The change in the irradiance profile is shown for 2 instances in Figure 7.

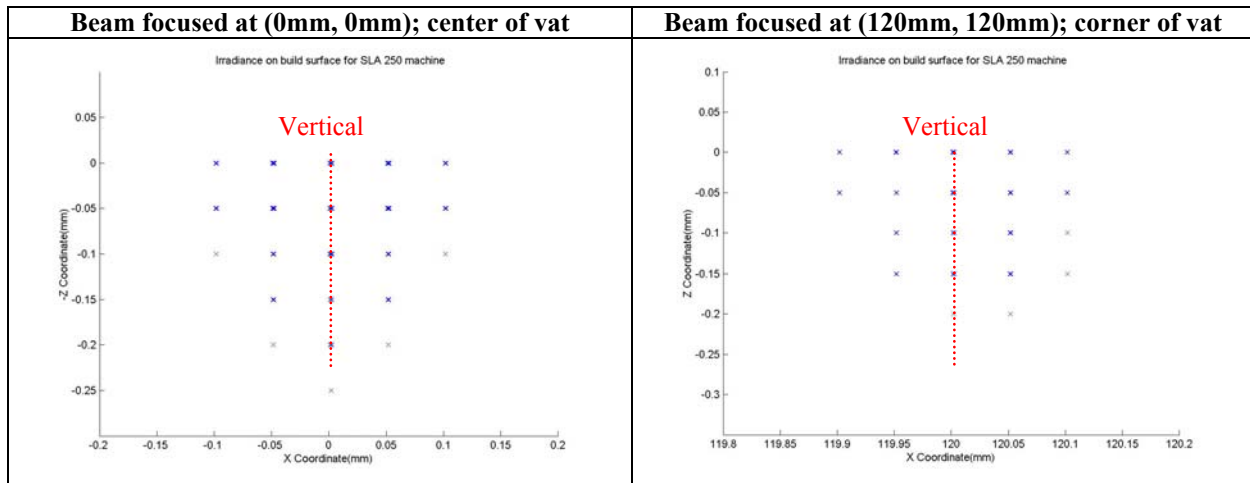


Figure 7. Change in shape of irradiance profile around focus point in the vat

As shown in Figure 7, the irradiance profile is symmetric about the vertical axis when the beam is focused at center of the vat. On the other hand, the profile is not only asymmetric about the vertical axis but also possesses a shorter reach at the corner of the vat. The ability of the analytical irradiance model to accurately predict the slanted nature of the laser beam is an important step in using this model to simulate build shapes. Therefore, it is possible to extend the equation further to calculate the exposure and curing characteristics of the resin over a given period of time.

3.2 Cure Profile Simulation

The analytical irradiance model forms the basis for predicting the exposure at any point in the vat. Upon calculation of exposure at a particular point, this exposure value is compared to the critical exposure value, E_c , above which a point is cured. In doing so, E_c , which is a resin constant, is taken as a meaningful threshold.

Direct integration of Equation 18 is not possible using Equation 17 since irradiance is not only a function of time, but space as well. Therefore, a suitable numerical integration method must be chosen to evaluate this integral. For this research, Simpson's 3/8 rule was chosen for numerical integration of exposure.

This numerical integration technique was applied to simulate the build process in a SLA250/50 machine using DSM Somos 7110 resin, which has an E_c value of 8.2 mJ/cm^2 and a D_p value of 0.14 mm. The cure profile for a 10 mm long line was simulated at 2 locations in the vat: one at the vat center where the y coordinate is 0 mm, and one at the edge of the vat, where the y coordinate is 120 mm. The comparison of the simulated line shapes is shown in Figure 8.

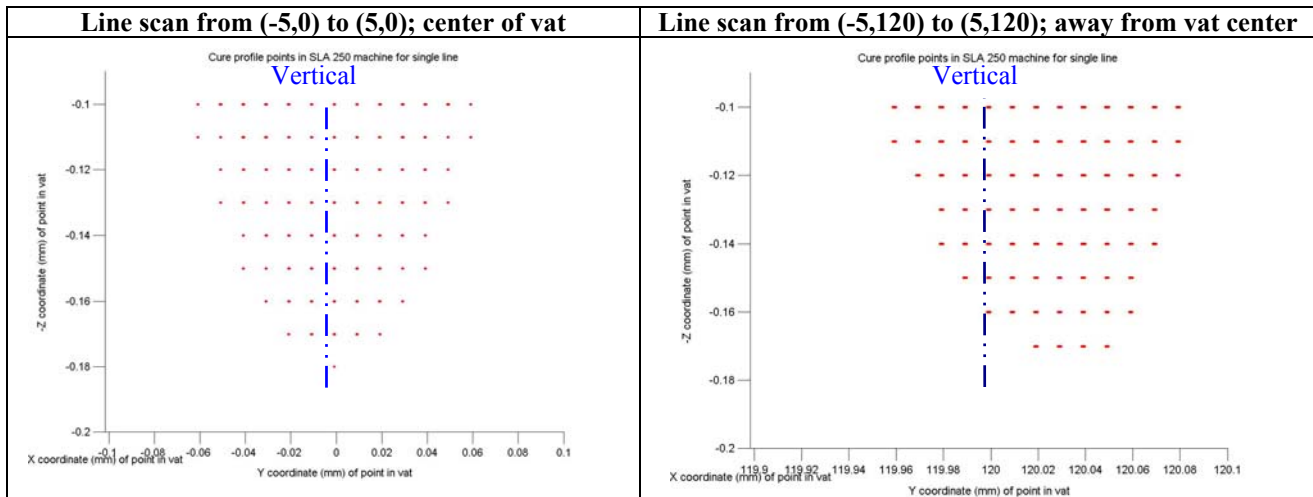


Figure 8. Change in shape of cure profile around scan line in the vat

In Figure 8, the direction of scan line is into the paper and the points represent cured points in the vat. Only the bottom surface of the cured profile is shown with the depth representing the depth into the vat. The axis is vertical through the point of intersection of laser beam with vat surface. As shown, the cured profile is symmetric about the vertical axis when the line is scanned at the center of the vat. On the other hand, the cure profile is slanted when the line is 120mm away from vat center.

In this line scan example, a scan speed of 750 mm/s was used, which is typical for the SLA250/50 machine. For this machine and resin combination, using the scan speed of 750 mm/s would result in an expected cure depth of 0.180 mm for a single line based on the traditional SLA cure model outlined in Table 1. Based on the same traditional model, the expected cured line width is 0.2 mm[1].

It is seen from Figure 8 that the simulated cure depth at the center of the vat is 0.18 mm. Closer examination with a finer grid still yielded the cure depth of 0.18 mm, which is in agreement with the predicted value. Even though it is not shown in Figure 8, the simulated cured line width is 0.2 mm, which also agrees with the expected line width. Accurate prediction of the size and shape of the cured outline for one scan can be extended to two-dimensional profiles, provided that the laser beam path is known.

To demonstrate this, a single-layer, 10 mm by 2mm horizontal area scan was simulated using 20 parallel, 10 mm long lines. A typical hatch spacing of 0.1 mm was used to ensure overlapping of scans. In Figure 9, the cure shape of this area is shown.

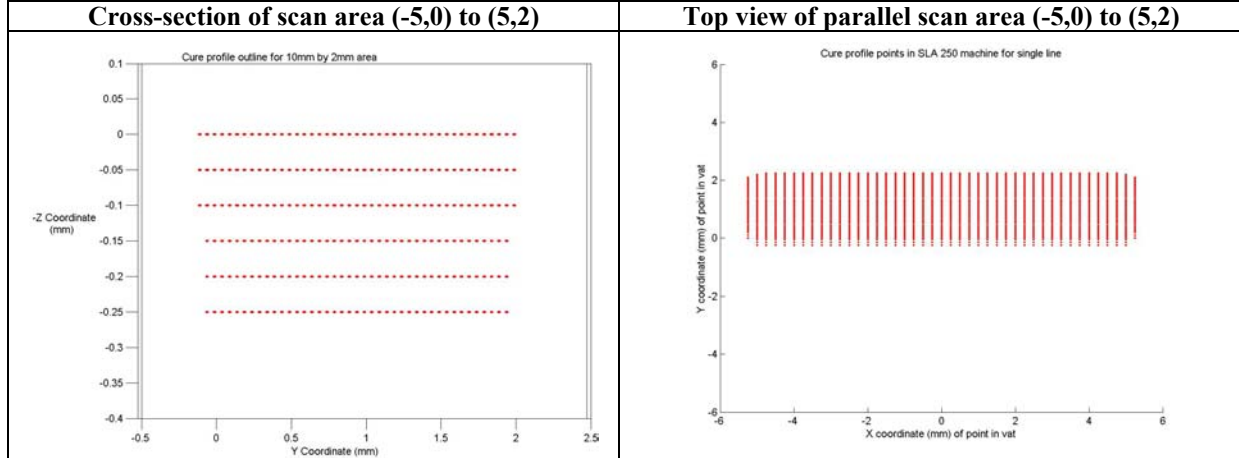


Figure 9. Cure area simulated by parallel overlapping scans

As seen in Figure 9, the cure profile of overlapping parallel scans yields a rectangular shape. In the cross-sectional view, the grid locations where curing occurs are shown. Using a finer grid would result in a better approximation of the cured profile; however, it is still seen that the width of the cured layer is almost uniform through a depth of 0.25mm. In fact, upon further increasing of mesh density, it was recorded that the depth of cure for this 2-dimensional, single-layer profile was 0.283 mm.

For multiple overlapping scans, the increase in the resulting cure depth is determined by the ratio of hatch spacing over beam waist diameter. For this example, this ratio was 0.8, which would result in a cure depth of 0.2826 mm [2] for overlapping scans. Again, the simulated results are quantitatively in agreement with predicted cure depth values.

In Figure 9, it is seen that at the corners of the rectangle, the cure profile tapers off, which is an expected result at the end of the scan lines. Since the scanned area was at the center of the vat and there were several overlapping scans, the surface finish is fairly even. However, for areas scanned far away from the center of the vat, the bumps in the surface finish would be more pronounced.

3.3 Surface Finish Quantification and Improvement

As aforementioned, scanning of an area at various locations in the vat yields parts with varying downfacing surface finish. If this change in surface finish can be quantified, then it could be corrected using process planning. An example of this is given by modifying the scan speed for an area scan in Figure 10. In Figure 10, the area scan shown in Figure 9 is simulated at a distance 120 mm away from the center of the vat and the resulting cure profile is plotted.

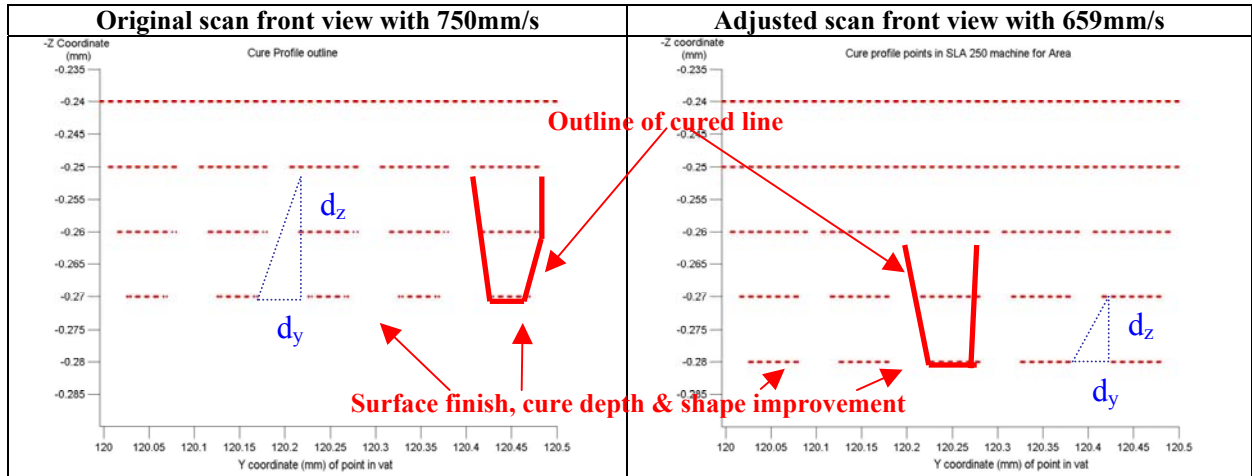


Figure 10. Surface finish improvement via adjusting scan speed

In Figure 10, the outline of cured lines is shown for each case. At the distance of 120 mm away from vat center, the cure depth of the resulting profile, when scanned with 750 mm/s, was simulated as 0.27 mm, and slanted with an uneven surface. Considering the refracted beam path, $V_{new} = V_{vatcenter}(1 - \sin \varphi)$ was used with respect to the scan speed at center of vat to adjust the scanning speed. In this case, the adjusted speed was calculated as 659 mm/s. When this new scan speed was used, the downfacing cure profile depth increased to 0.28mm, which was the cure depth value at center of vat, and the cure profile became more uniform, as shown in Figure 10.

The parameters d_y and d_z in Figure 10 represent a simple means of quantifying surface finish. Quantification of d_y and d_z means documentation of the surface finish for downfacing surfaces. In the future, the surface finish will be computed using one of the established metrics such as Ra or RMS. The capability to improve surface finish by adjusting only one parameter has been demonstrated in Figure 10. If the number of SLA process parameters that have a bearing on surface finish are considered, we can see that this capability can be further extended within process planning.

Surface finish quantification is also valuable for SLA machine parameter estimation. Simply put, instead of predicting the outline of a cure profile based on SLA process parameters, the desired surface finish can be expressed as an equation whose variables are the various laser beam and scanning parameters. Furthermore, surface finish, i.e. cure profile, is directly related to the exposure received at a particular point of interest. Since exposure is a function of resin, scan pattern, laser beam (irradiance, diameter, and angle with vertical), and location parameters, it can be expressed as:

$$E_{point} = E(D_p, \eta, H, H_o, \theta, \gamma, \lambda, f, h_s, LT, x, y, z, t) \quad (\text{Equation 19})$$

Equation 19 contains several parameters that the exposure is dependent on. For better surface finish, the goal is to have the points along the desired cure profile to be at or above the critical exposure value. Since the goal is to minimize the deviation of exposure at any point from the critical exposure this could be treated as a least squares minimization problem. Thus, this optimization problem with multiple parameters can be solved to yield combination of parameter values or ranges that will give the desired exposure value, i.e. minimize Ra or RMS. In short, the

analytical model presented here will be used within parameter estimation as part of process planning to improve surface finish.

4. DISCUSSION AND FUTURE WORK

In this paper, a new analytical irradiance model for the SLA process is presented. The model presented here is only a start aimed at improving SLA surface finish. This analytical model is an improvement over existing models, because it accounts for dynamic laser beam parameters. Using this model along with numerical methods, the outline of cure profiles has been simulated. Simulation results agree with existing theoretical models for SLA cure modeling. So far, only one-layer cure profiles have been simulated. However, SLA parts are three-dimensional, consisting of multiple layers with different scan patterns. In order to experimentally validate the model presented here, multiple-layer parts' cure profiles need to be simulated.

Using cure profile results from the presented model, it is possible to characterize SLA process planning as a parameter estimation problem for design of different SLA machine configurations. To achieve this, standard metrics for surface finish quantification will be used.

As part of ongoing work, the least squares minimization problem for exposure is being formulated. Since exposure is a function of many parameters, it is conceivable that no suitable combination of these parameters can be achieved within the available design space. However, certain assumptions about resin and laser beam behavior will be made, which will simplify the problem at hand, making it a solvable one.

ACKNOWLEDGEMENTS

We gratefully acknowledge the support from the Rapid Prototyping and Manufacturing Institute member companies and the George W. Woodruff School of Mechanical Engineering at Georgia Tech.

REFERENCES

1. Jacobs, P.F., *Rapid Prototyping & Manufacturing: Fundamentals of Stereolithography*. 1992: Society of Manufacturing Engineers.
2. Jacobs, P.F., *Stereolithography and other RP&M Technologies: from Rapid Prototyping to Rapid Tooling*. 1996: Society of Manufacturing Engineers.
3. Reeves, P.E. and R.C. Cobb, *Reducing the surface deviation of stereolithography using in-process techniques*. *Rapid Prototyping Journal*, 1997. **3**(1): p. 20-31.
4. Lu, L., J.Y.H. Fuh, and Y.S. Wong, *Laser-Induced Materials and Processes for Rapid Prototyping*. 2001: Kluwer Academic Publishers. 267.
5. Sambu, S.P. 2001. "A Design For Manufacturing Method for Rapid Prototyping and Rapid Tooling," *Master's Thesis, Mechanical Engineering*, Georgia Institute of Technology, Atlanta, GA.
6. Kataria, A. and D.W. Rosen. *Building Around Inserts: Methods for Fabricating Complex Devices in Stereolithography*. in *ASME DETC*. 2000. Baltimore, MD: ASME.
7. O'Shea, D.C., *Elements of Modern Optical Design*. 1985: John Wiley and Sons.
8. Partanen, J., *3D Systems Inc*. 2002.
9. Flach, L. and R.P. Chartoff, *A Process Model for Nonisothermal Photopolymerization with a Laser Light Source I: Basic Model Development*. *Polymer Engineering and Science*, 1995. **35**(6): p. 483-492.
10. Flach, L. and R.P. Chartoff, *A Process Model for Nonisothermal Photopolymerization with a Laser Light Source II: Behavior in the Vicinity of a Moving Exposed Region*. *Polymer Engineering and Science*, 1995. **35**(6): p. 493-498.
11. Narahara, H. and K. Saito. *Fundamental Analysis of Single Layer Created by Three Dimensional Photofabrication*. in *International Conference on Rapid Prototyping*. 1994. Dayton, OH: University of Dayton.
12. Edwards, C.H. and D.E. Penney, *Calculus with Analytic Geometry*. 4th ed. 1994, Englewood Cliffs, NJ: Prentice-Hall Inc.